TOPOLOGICAL NATURE OF MULTI-WEYL SEMIMETALS

M.Sc. Project Report

M.Sc. Physics

Indian Institute of Technology Indore

Author: Pawan Kumar Yadav

Roll No: 2303151023

Supervisor: Dr. Alestin Mawrie

Indian Institute of Technology Indore

CANDIDATE'S DECLARATION

I hereby certify that the work which is being presented in the thesis entitled **Topological nature of multi-Weyl semimetals** in the fulfillment of the requirements for the award of the degree of **MASTER OF SCIENCE** and submitted in the **DISCIPLINE OF PHYSICS**, Indian Institute of Technology Indore, is an authentic record of my own work carried out during the time period from **August 2024** to **May 2025** under the supervision of **Alestin Mawrie, IIT Indore, Department of Physics** The matter presented in this thesis has not been submitted by me for the award of any other degree of this or any other institute.

Signature of the student

(Pawan Kumar Yadav)

. . . . . .

This is to certify that the above statement made by the candidate is correct to the best of my knowledge.

Signature of the Supervisc

(Alestin Mawrie)

. . . . . .

Pawan Kumar Yadav has successfully given his M.Sc. Oral Examination held on **13 May, 2025**.

. . . . . .

Signature of Supervisor of MSc thesis

Date:

Convener, DPGC

Date: 26-05-25

Contents

Contents **1**

1 Introduction **1**

2 Adiabatic Theorem **6**

2.1 Adiabatic process 6

2.2 proof of adiabatic theorem 8

3 Berry's Phase **11**

3.1 Classical example 11

3.2 Geometric Phase 12

3.3 Berry phase as magnetic flux 14

4 The Aharonov-Bohm Effect **16**

4.1 Theory 16

4.2 Aharonov-Bohm effect as Berry's phase 19

5 About the mono-pole Weyl semi-metal **21**

5.1 Weyl Semimetals and the Concept of Monopoles 21

5.1.1 Chiral Partner of a Weyl Point 22

6 Formulation of multi-Weyl semi-metal **25**

6.1 Hamiltonian of a multi-Weyl semi-metal 25

6.2 The Berry curvature field 27

7 Landau Levels and their degeneracy **30**

7.1 Landau level 30

7.2 Landau level of gas 31

7.3 Degeneracy calculation 33

8 Landau level calculation of hamiltonian **34**

8.1 Hamiltonian of a multi-Weyl semi-metal 34

8.2 Landau levels of the hamiltonian 35

9 Chiral Anomaly **38**

9.1 Chiral anomaly of Landau levels 39

10 Conclusion **40**

Bibliography **41**

Abstract

Berry curvature in Weyl semimetals plays a critical role in shaping the topological properties and electronic transport phenomena of these materials. Weyl semimetals, characterized by the presence of Weyl nodes (monopoles of Berry curvature) show unique features such as Fermi arcs on their surface and non-trivial responses to external fields. This report provides a brief overview of the concept of Berry curvature in the context of Weyl semimetals, discussing its emergence from the topology of the electronic band structure and its influence on various physical observables, such as the anomalous Hall effect, chiral anomaly, and magneto-resistance. The role of Berry curvature in mediating the dynamics of charge carriers, particularly its effect on the velocity and current response of electrons near the Weyl nodes, is also explored.

Landau quantization comes from charged particles occupying quantized energy levels in presence of magnetic field. It is mainly studied in reference of the two-dimensional electron gas. When electron are placed in magnetic field then motion is restricted in plane perpendicular to magnetic field. Energy associated with Landau level is like harmonic oscillator in quantum mechanics. Landau levels help understand Quantum hall effect where conductance in $2d$ electron gas becomes quantized.

Chapter 1

Introduction

In the context of materials science, Weyl semimetals are materials that feature Weyl fermions as low-energy excitations. They are characterized by the following key features:

- Weyl Points (Topological Singularities): Weyl semimetals host points in their momentum space, called Weyl nodes, where the conduction and valence bands meet. At these points, the energy bands act like Weyl fermions, which are massless and have a linear energy-momentum relationship. These Weyl nodes can be thought of as "monopoles" in momentum space, where the chirality (or handedness) of the fermions is either left-handed or right-handed. These nodes typically appear in pairs, one with positive chirality and the other with negative chirality.

- Chirality: The concept of chirality (or handedness) is essential in Weyl semimetals. The electrons near the Weyl nodes behave like massless Weyl fermions and can have a distinct left- handed (negative chirality) or right-handed (positive chirality) orientation. This leads to phenomena such as the chiral anomaly, where the number of right-handed and left-handed particles can change under certain conditions, especially in the presence of electromagnetic fields.

- Topological Nature: Weyl semimetals are considered topologically nontrivial materials because of their unique band structures. The topological protection leads to robust surface states (called Fermi arcs) that connect the projections of the Weyl nodes on the surface of the material. Fermi arcs are linked to the Weyl nodes in momentum space and often appear as arcs on the surface of the material. These surface states are often highly conducting and can be sensitive to external perturbations, making Weyl semimetals interesting for applications in electronics and quantum devices.

- Anomalous Transport Phenomena: Weyl semimetals can exhibit unusual transport properties, such as: Chiral anomaly: Under parallel electric and magnetic fields, the number of right- and left-handed Weyl fermions can change, leading to an unusual form of the current generation. Negative magnetoresistance: The material's resistance decreases in the presence of a magnetic field.

- Materials: Several materials have been identified or predicted to behave as Weyl semimetals. Some of the known examples include: TaAs (Tantalum arsenide) NbAs (Niobium arsenide) Cd_3As_2 (Cadmium arsenide) WTe_2 (Tungsten telluride) These materials have been experimentally studied and found to exhibit Weyl semimetal characteristics, such as surface Fermi arcs and unusual transport phenomena.

Weyl semimetals are of great interest for their potential applications in areas such as (to name a few):

- Quantum computing: Their topologically protected surface states could play a role in quantum information processing. Next-generation electronics: The chiral anomaly and unusual transport properties could lead to new types of electronic devices.

- Spintronics: The manipulation of electron spins might be enhanced due to the unique behavior of Weyl fermions.

In short Weyl semimetals are fascinating materials where the electron behavior is dominated by the physics of massless Weyl fermions. Their unique electronic structures, topological properties, and potential for new quantum phenomena make them an exciting area of research in condensed matter physics and materials science.

In this report, we stress on the multi-Weyl semimetal (mWSM)[1, 2, 3] which is an exotic phase of matter where Weyl nodes—points of band-touching in momentum space—carry a topological charge greater than one. This higher monopole charge, $|m| > 1$, differentiates multi-Weyl semimetals from conventional Weyl semimetals (WSMs),[4, 5, 6] in which nodes act as Berry curvature monopoles with charge ± 1. As a result, mWSMs exhibit unique Berry curvature distributions and dispersion relations around each Weyl node, leading to novel physical properties.

Additionally, we observed an enhanced Berry curvature field due to the higher monopole charges in mWSMs, which leads to pronounced anisotropy in optical conductivity. This field intensifies interband transitions near the Weyl nodes, resulting in a frequency-dependent optical conductivity with directional selectivity. The singularity in the optical Hall conductivity at specific frequencies, observed only for $m = 1$, highlights a resonance-like behavior absent in systems with $m = 2$ or 3. Higher monopole charges distribute the Berry curvature more broadly around the nodes, enabling tunable, anisotropic optical responses beneficial for polarization-sensitive photodetectors and frequency-selective devices.

The remainder of the thesis is organized as follows:

In Chapter 2, we discuss the adiabatic process. When the Hamiltonian varies slowly from some initial value to a final value with time dependence. The initial state is an eigenstate of Hamiltonian and is non-degenerate. We prove the adiabatic theorem, which is necessary for calculating the extra phase obtained by the wave function.

In Chapter 3, we discuss the Berry phase and how we can derive it from a given

Hamiltonian. First we take a classical example to describe non-holonomic process and then we go quantum for some particular Hamiltonian. We take slowly varying Hamiltonian and calculate it's eigenfunction. As we will observe we get some phase factor in addition to the phase we get from time independent hamiltonian. After that we try to correspond Berry's phase with magnetic flux using Stokes's theorem.

In Chapter 4, we gave an example of Berry's phase which is Aharonov-Bohm effect. We put magnetic and electric field in Hamiltonian for that we take scaler and vector potential and use gauge to change those potential to our convenience. We solve the Hamiltonian equation and get some phase factor. Now to se this as Berry's phase we take a particle trapped in a box outside a solenoid. There is some potential because of that solenoid and we are going to move the box around the solenoid. Now the centre of box is varying slowly so it is an adiabatic process and we try to solve the Hamiltonian. The curl is time independent. After that the phase obtained is equates with Berry's phase.

In Chapter 5, we discuss the monopole Weyl semimetal, and how touching of conduction and valence bands at discrete points in momentum space give Weyl nodes. We see how the Berry curvature field in momentum space can be written mathematically, and also define the Berry connection. We also discuss that there is a chiral partner to every Weyl node with opposite chirality. These nodes are separated in momentum space. We talk about Fermi arcs, which are an open surface-state band structure. We also discuss transport properties and some examples of materials that show these phenomena.

In Chapter 6, we discussed in previous chapter generalize the Weyl nodes and consider more than one. We take a particular Hamiltonian of multi-Weyl semimetal and calculate it's eigenstate. We also talk about some addition part of that Hamiltonian known as tilt. There is linear tilt and quadratic tilt components which can modify the dispersion relation. From the eigenstates we calculated we get Berry connection and from that we get Berry curvature. We plot these Berry curvature

field for different values of topological charges.

In Chapter 7, we discuss Landau levels and how putting magnetic field perpendicular to 2D electron or charge gas changes its energy levels. These energy are same as harmonic oscillator from quantum mechanics with cyclotron frequency. After that we derive that formula by taking hamiltonian of free gas and putting magnetic field in that. The energy levels calculated here have degeneracy we calculate that by taking some sample size and we get a flux quanta number.

In Chapter 8, here as discussed previously we use that multi-Weyl hamiltonian for its Landau level calculation. First we need to modify this Hamiltonian for easier calculation. We put vector potential for the magnetic field and transform the momentum to general momentum. We take new operators known as creation and annihilation operators and we modify the Hamiltonian it will look similar to harmonic oscillator. Now we calculate its energy levels and eigen wave function which will be different for different values of energy level depending on if the energy level is smaller of bigger then number of Weyl nodes.

In Chapter 9, we talk about Chiral anomaly arising from electric or magnetic field presence in that Hamiltonian. That field breaks the chiral symmetry and gives non-conservation law of chiral charge, which leads to transport phenomena. We discuss how it affects different phenomena and some examples of material which show this. We also discuss how chirality can be detected by optical detection. Then when electric and magnetic field applied parallel it affects inequality of population between Landau levels with opposite chirality.

Chapter 2

Adiabatic Theorem

2.1 Adiabatic process

In an ideal pendulum, when you slowly and smoothly shift the support, the pendulum will still swing back and forth smoothly in the same plane with the same amplitude. It is this slow change in external conditions that characterizes an adiabatic process.

There are two important times to think about: T_i, the "internal" time, which is the time for the pendulum's oscillations, and T_e, the "external" time, which is the timescale on which external parameters change appreciably—such as the period of an oscillating platform on which the pendulum is mounted. An adiabatic process takes place when changes in external circumstances occur slowly relative to the internal evolution of the system. An adiabatic process is one for which $T_e \gg T_i$.. To examine an adiabatic process, the usual method is to first solve the system with the outside parameters fixed. Having determined the behavior of the system in these fixed conditions, you can then add the slow changes in these parameters. There are numerous such examples for adiabatic approximation such as Born-Oppenheimer approximation.

In quantum mechanics, the adiabatic approximation is contained in the adiabatic theorem. According to this theorem, if the Hamiltonian of a system varies

slowly from an initial form H^i to a final form H^f, then if a particle is initially in the nth eigenstate of H^i it will always be in the corresponding nth eigenstate of H^f during the evolution, provided that the transitions are slow enough and the system is not degenerate.

In this scenario, we start with a particle in the ground state of an infinite square well, described by the wave function:

$$\psi^i(x) = \sqrt{\frac{2}{a}} \sin\left(\frac{\pi}{a}x\right) \tag{2.1}$$

If we slowly shift the right wall of the well to $2a$, then the adiabatic theorem guarantees that the particle will evolve smoothly to the ground state of the new well, which is:

$$\psi^f(x) = \sqrt{\frac{1}{a}} \sin\left(\frac{\pi}{2a}x\right) \tag{2.2}$$

This transition occurs smoothly because the change in the Hamiltonian is slow, allowing the system to adapt to the new conditions.

But if the wall expands abruptly, the state is now $\psi^i(x)$, which is a superposition of the eigenstates of the new Hamiltonian for the expanded well. The abrupt transition violates the smooth evolution under specific conditions established by the adiabatic theorem and results in a more complicated state following the expansion.

When the right wall of the infinite square well expands at a constant velocity v, the complete set of solutions can be expressed as:

$$\Phi_n(x,t) \equiv \sqrt{\frac{2}{w}} \sin\left(\frac{n\pi}{w}x\right) e^{i\left(mvx^2 - 2E'_n at\right)/2\hbar w} \tag{2.3}$$

Here, $w(t) \equiv a + vt$ tells the width of well at time t, and $E_n^i \equiv n^2\pi^2\hbar^2/2ma^2$ is the energy of the nth state in the initial configuration.

The general solution can be given by linear combination of the Φ 's:

$$\Psi(x,t) = \sum_{n=1}^{\infty} c_n \Phi_n(x,t) \tag{2.4}$$

This framework allows for an exact solution, capturing the dynamics of the particle as the well expands, and illustrates the difference between adiabatic and sudden changes in quantum systems.

The phase factor in $\Psi(x,t)$ can be written as

$$\theta(t) = -\frac{1}{\hbar}\int_0^t E_1\left(t'\right) dt' \tag{2.5}$$

here $E_n(t) \equiv n^2\pi^2\hbar^2/2mw^2$ is the nth instantaneous eigenvalue, at instantaneous time t.

2.2 proof of adiabatic theorem

If the time-dependent Hamiltonian can be expressed by equation:

$$H'(t) = Vf(t) \tag{2.6}$$

where V is some potential and $f(t)$ is a time-dependent function that begins zero (at $t = 0$) and ramps up to 1 (at $t = T$), this formulation enables us to explore how the potential influences the system dynamics with respect to time. Suppose that the particle is initially in the nth eigenstate of the initial Hamiltonian:

$$\Psi(0) = \psi_n^i \tag{2.7}$$

and transform into some state $\Psi(t)$. We must show that

$$\left|\left\langle \Psi(T) \mid \psi_m^f \right\rangle\right|^2 = \begin{cases} 1, & \text{for } \ m = n \\ 0, & \text{for } m \neq n \end{cases} \tag{2.8}$$

In the context of first-order time-independent perturbation theory, we can determine the final state ψ_m^f of a quantum system after a slow, time-dependent change in the Hamiltonian.

first-order time-dependent perturbation, we can analyze how a quantum state evolves under the influence of a time-dependent Hamiltonian, so we solve for $\Psi(T)$.

$$\Psi(t) = \sum_l c_l(t)\psi_l e^{-iE_l t/\hbar} \tag{2.9}$$

where

$$c_n(t) \cong 1 - \frac{i}{\hbar} V_{nn} \int_0^t f\left(t'\right) dt' \tag{2.10}$$

will give

$$c_l(t) \cong -\frac{V_{ln}}{E_l - E_n} \left\{ f(t) e^{i(E_l - E_n)t/\hbar} - \int_0^t \frac{df}{dt'} e^{i(E_l - E_n)t'/\hbar} dt' \right\}.$$

In the adiabatic approximation, where we need the function $f(t)$ to change very slowly over time, such that the rate of change df/dt is extremely small compared to the intrinsic frequencies of the system. We assume that

$$\frac{df}{dt} \ll \frac{|E_l - E_n|}{\hbar} f \tag{2.11}$$

exploring the orthonormality of initial eigenfunctions, we get that

$$\left\langle \Psi(T) \mid \psi_m^f \right\rangle = \begin{cases} \left[1 + i\frac{V_{nn}A}{\hbar}\right] e^{iE_n T/\hbar}, & m = n \\ 0 & m \neq n \end{cases} \tag{10.19}$$

This shows when both the adiabatic condition and the smallness of the perturbation are satisfied, the quantum system remains in its original eigenstate, with no significant transitions occurring to other states.

Chapter 3

Berry's Phase

3.1 Classical example

Berry's phase or the geometric phase is a basic principle in physics explaining how the wavefunction of a system gains a phase factor as it adiabatically (slow and reversible) evolves in parameter space in a closed loop. Although frequently debated in quantum mechanics, there are classical analogs to Berry's phase that demonstrate its concepts in more intuitive contexts.

Perhaps the most famous classical analogue of Berry's phase is the Hannay angle, which appears in systems parametrized by action-angle coordinates. When a classical system evolves adiabatically and in a cycle for its parameters, the phase shift of the angle variable corresponding to the action variable is obtained, a classical analogue to Berry's phase in quantum systems. This phenomenon can be seen most clearly in systems such as the Foucault pendulum, in which the plane of oscillation turns as a consequence of the Earth's rotation, showing a classic example of the geometric phase.

In classical systems, Berry's phase can be visualized by considering a system's trajectory in parameter space. As the system evolves along a closed loop, the accumulated phase shift can be observed, providing insight into the geometric nature of the phase. This visualization helps bridge the gap between the abstract

concept of Berry's phase and tangible classical systems.

Understanding these classical examples not only deepens our comprehension of Berry's phase but also highlights the interconnectedness of classical and quantum physics. If you're interested in exploring more about Berry's phase or its applications in various fields.

Section area on earth is $A = (1/2)(\Theta/2\pi)4\pi R^2 = \Theta R^2$ (here R is the radius of earth).

So Θ only depends on solid angle and is independent of the path. The solid angle subtended by a latitude line θ_0 is

$$\Omega = 2\pi\,(1 - \cos\theta_0) \tag{3.1}$$

3.2 Geometric Phase

To investigate the quantum mechanics of adiabatic, nonholonomic processes. The question one wants to answer is the following: When the parameters in the Hamiltonian are adiabatically carried about some closed loop, how is the final state different from the initial state?

If the Hamiltonian does not depend on time, then a particle that begins in the nth eigenstate $\psi_n(x)$

$H\psi_n(x) = E_n\psi_n(x)$ remains in the nth eigenstate, only picking up phase factor:

$$\Psi_n(x,t) = \psi_n(x)e^{-iE_nt/\hbar} \tag{3.2}$$

If Hamiltonian changed with time, then the eigenfunctions and eigenvalues will be time dependent:

$$H(t)\psi_n(x,t) = E_n(t)\psi_n(x,t) \tag{3.3}$$

Adiabatic theorem informs us that as H varies extremely slowly, a particle

which is initially in the nth eigenstate will stay in the nth eigenstate-acquiring at most a time-dependent phase factor-even as the eigenfunction itself changes.

$$\Psi_n(x,t) = \psi_n(x,t) e^{-\frac{i}{\hbar}\int_0^t E_n(t')dt'} e^{i\gamma_n(t)} \tag{3.4}$$

The term

$$\theta_n(t) \equiv -\frac{1}{\hbar}\int_0^t E_n(t')\,dt' \tag{3.5}$$

known as the dynamic phase; it generalizes the "standard" factor $(-E_n t/\hbar)$ to where E_n is a function of time. Any "extra" phase, $\gamma_n(t)$, is geometric phase. Normalization condition only determine $\psi_n(x,t)$ up to an arbitrary phase, since this arbitrary phase could in principle be chosen independently at each instant of time we have to allow for an arbitrary phase factor.

The Schrödinger equation,

$$i\hbar\frac{\partial\Psi}{\partial t} = H(t)\Psi \tag{3.6}$$

inner product with ψ_n and normalized wave form give solution as

$$\frac{d\gamma_n}{dt} = i\left\langle \psi_n \middle| \frac{\partial\psi_n}{\partial t} \right\rangle \tag{3.7}$$

Now $\psi_n(x,t)$ depends on time t because there is parameter $R(t)$ in the Hamiltonian which changes with time gives

$$\frac{d\gamma_n}{dt} = i\left\langle \psi_n \middle| \frac{\partial\psi_n}{\partial R} \right\rangle \frac{dR}{dt}$$

hence

$$\gamma_n(t) = i\int_{R_i}^{R_f} \left\langle \psi_n \middle| \frac{\partial\psi_n}{\partial R} \right\rangle dR \tag{3.8}$$

here R_i and R_f give initial and final values of $R(t)$.

In case Hamiltonian goes back to its original form after time T, which will give $R_f = R_i$, then $\gamma_n(T) = 0$ if there is only one parameter.

Let's say there are N number of them: $R_1(t), R_2(t), \ldots, R_N(t)$; in that case

$$\frac{\partial \psi_n}{\partial t} = \frac{\partial \psi_n}{\partial R_1}\frac{dR_1}{dt} + \frac{\partial \psi_n}{\partial R_2}\frac{dR_2}{dt} + \cdots + \frac{\partial \psi_n}{\partial R_N}\frac{dR_N}{dt} = (\nabla_R \psi_n) \cdot \frac{d\mathbf{R}}{dt} \tag{3.9}$$

if the Hamiltonian goes back to its original form after a time T, the net geometric phase change is

$$\gamma_n(T) = i \oint \langle \psi_n \mid \nabla_R \psi_n \rangle \cdot d\mathbf{R} \tag{3.10}$$

here $\gamma_n(T)$ is called Berry's phase and it's real. Geometric phase will vanish whenever the eigenfunctions of $H(t)$ are real.

3.3 Berry phase as magnetic flux

This phase carries a deep analogy with magnetic flux, especially within the realm of gauge theories and electromagnetism. In electromagnetism, the vector potential A leads to the magnetic field B via the curl operation:

$$\Phi \equiv \int_S \mathbf{B} \cdot d\mathbf{a} \tag{3.11}$$

when we write magnetic field in terms of vector potential ($\mathbf{B} = \nabla \times \mathbf{A}$), and after applying Stokes' theorem:

$$\Phi = \oint_C \mathbf{A} \cdot d\mathbf{r} \tag{3.12}$$

Berry's phase can be considered as the "flux" of a "magnetic field". This integral is path-independent and solely depends on the enclosed flux, similar to the case

of magnetic flux in electromagnetism. The gauge invariance of the Berry phase guarantees that only the enclosed flux enters the phase, and not the particular path used.

$$\mathrm{B} = i\nabla_R \times \langle \psi_n \mid \nabla_R \psi_n \rangle \tag{3.13}$$

by closed-loop trajectory in parameter space. In the three-dimensional situation, then, Berry's phase is a surface integral,

$$\gamma_n(T) = i \int [\nabla_R \times \langle \psi_n \mid \nabla_R \psi_n \rangle] \cdot d\mathbf{a} \tag{3.14}$$

The analogy between Berry's phase and magnetic flux thus offers a profound insight into the geometric origin of quantum phases. In just the way that magnetic flux affects the phase of a charged particle's wavefunction, the Berry curvature in parameter space affects the phase of a system's state, highlighting the fundamental relationship between geometry and physics.

Chapter 4

The Aharonov-Bohm Effect

4.1 Theory

In electrodynamics the potentials φ and $\mathbf{A}$ can not be directly measured, the physical quantities are electric and magnetic fields:

$$\mathbf{E} = -\nabla\varphi - \frac{\partial \mathbf{A}}{\partial t}, \quad \mathbf{B} = \nabla \times \mathbf{A} \tag{4.1}$$

we are perfectly free to change the potentials from gauge:

$$\varphi \to \varphi' = \varphi - \frac{\partial \Lambda}{\partial t}, \quad \mathbf{A} \to \mathbf{A}' = \mathbf{A} + \nabla\Lambda \tag{4.2}$$

where Λ is some function of position and time and this is a gauge transformation, and it has no influence whatever on the fields.

But in quantum mechanics the potentials have a greater importance, for the Hamiltonian is given in terms of φ and $\mathbf{A}$, not $\mathbf{E}$ and $\mathbf{B}$:

$$H = \frac{1}{2m}\left(\frac{\hbar}{i}\nabla - q\mathbf{A}\right)^2 + q\varphi \tag{4.3}$$

still theory will not change under Gauge transformation.

Aharonov and Bohm demonstrated that the vector potential can influence the

quantum properties of a charged particle that never experiences an electromagnetic field.

Consider a particle that is confined to travel in a circle of radius b. On the axis is a solenoid of radius $a < b$, with a magnetic field $\mathbf{B}$ .If the solenoid is very long, the field inside is uniform and the outside is zero. But the vector potential outside the solenoid is not zero; indeed (using the convenient gauge condition $\nabla \cdot \mathbf{A} = 0$)

$$\mathbf{A} = \frac{\Phi}{2\pi r}\hat{\phi}, \quad (r > a) \tag{4.4}$$

where $\Phi = \pi a^2 B$ is the magnetic flux through the solenoid. On the other hand, the solenoid is uncharged, and thus the scalar potential φ equals zero. In this situation the Hamiltonian is

$$H = \frac{1}{2m}\left[-\hbar^2\nabla^2 + q^2A^2 + 2i\hbar q\mathbf{A}\cdot\nabla\right] \tag{4.5}$$

The wave function depends on the azimuthal angle $\phi, (\theta = \pi/2$ and $r = b)$ so $\nabla \to (\hat{\phi}/b)(d/d\phi)$, and the Schrödinger equation is

$$\frac{1}{2m}\left[-\frac{\hbar^2}{b^2}\frac{d^2}{d\phi^2} + \left(\frac{q\Phi}{2\pi b}\right)^2 + i\frac{\hbar q\Phi}{\pi b^2}\frac{d}{d\phi}\right]\psi(\phi) = E\psi(\phi) \tag{4.6}$$

here this is a linear differential equation with coefficients:

$$\frac{d^2\psi}{d\phi^2} - 2i\beta\frac{d\psi}{d\phi} + \epsilon\psi = 0 \tag{4.7}$$

and

$$\beta \equiv \frac{q\Phi}{2\pi\hbar} \quad \text{and} \quad \epsilon \equiv \frac{2mb^2E}{\hbar^2} - \beta^2 \tag{4.8}$$

solutions are as

$$\psi = Ae^{i\lambda\phi} \tag{4.9}$$

after solving

$$\lambda = \beta \pm \sqrt{\beta^2 + \epsilon} = \beta \pm \frac{b}{\hbar}\sqrt{2mE} \tag{4.10}$$

Continuity of $\psi(\phi)$, at $\phi = 2\pi$, needs that λ has to be an integer:

$$\beta \pm \frac{b}{\hbar}\sqrt{2mE} = n \tag{4.11}$$

and energy solution is

$$E_n = \frac{\hbar^2}{2mb^2}\left(n - \frac{q\Phi}{2\pi\hbar}\right)^2, \quad (n = 0, \pm 1, \pm 2, \ldots) \tag{4.12}$$

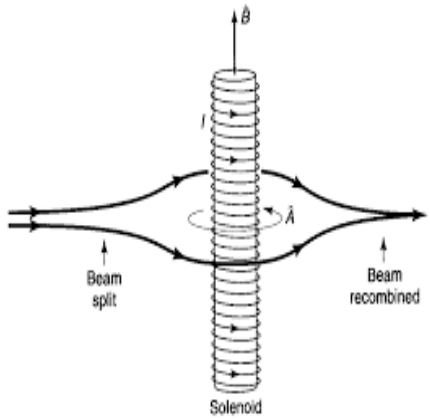

Figure 4.1: Aharonov-Bohm effect where beam passing around solenoid

Positive n, which is a particle moving in the same direction as the current in the solenoid, has a slightly lower energy (if q is negative) than negative n , which is a particle moving in the opposite direction. More importantly, the permissible energies clearly depend on the field inside the solenoid, even though the field at the location of the particle is zero. More broadly, assume that a particle is traveling in an area where $\mathbf{B}$ is zero (so $\nabla \times \mathbf{A} = 0$), but $\mathbf{A}$ itself is not. Now, changing the Ψ

$$\Psi = e^{ig}\Psi' \tag{4.13}$$

here

$$g(\mathbf{r}) \equiv \frac{q}{\hbar} \int_{\mathcal{O}}^{\mathbf{r}} \mathbf{A}\left(\mathbf{r}'\right) \cdot d\mathbf{r}' \tag{4.14}$$

The (time-dependent) Schrödinger equation will be

$$-\frac{\hbar^2}{2m} \nabla^2 \Psi' + V \Psi' = i\hbar \frac{\partial \Psi'}{\partial t} \tag{4.15}$$

Evidently Ψ' satisfies the Schrödinger equation in the absence of A. If you can solve it, fixing for the presence of a (curl-free) vector potential is easy: You simply add on the phase factor e^{ig}.

4.2 Aharonov-Bohm effect as Berry's phase

The Aharonov-Bohm effect can be seen as a manifestation of geometric phase. Assume the charged particle is trapped in a box (whose center lies at position $\mathbf{R}$ outside the solenoid) by a potential $V(\mathbf{r} - \mathbf{R})$. (We're going to move the box around the solenoid soon, so $\mathbf{R}$ will be time-dependent, but for the time being it is merely some fixed vector.) The eigenfunctions of the Hamiltonian are found by

$$\left\{ \frac{1}{2m} \left[\frac{\hbar}{i} \nabla - q\mathbf{A}(\mathbf{r}) \right]^2 + V(\mathbf{r} - \mathbf{R}) \right\} \psi_n = E_n \psi_n \tag{4.16}$$

We have already solved equations of this form by:

$$\psi_n = e^{ig} \psi_n' \tag{4.17}$$

observe that ψ_n' is a function of only the combination ($\mathbf{r} - \mathbf{R}$). Now we take the box around the solenoid (in this case there is no need for the process to be adiabatic). In order to find Berry's phase, we first need to calculate the amount

$\langle \psi_n \mid \nabla_R \psi_n \rangle$. Using

$$\nabla_R \psi_n = \nabla_R \left[e^{ig} \psi_n'(\mathbf{r} - \mathbf{R}) \right] = -i \frac{q}{\hbar} \mathbf{A}(\mathbf{R}) e^{ig} \psi_n'(\mathbf{r} - \mathbf{R}) + e^{ig} \nabla_R \psi_n'(\mathbf{r} - \mathbf{R})$$

we get

$$\langle \psi_n \mid \nabla_R \psi_n \rangle \; = -i \frac{q}{\hbar} \mathbf{A}(\mathbf{R}) - \int \left[\psi_n'(\mathbf{r} - \mathbf{R}) \right]^* \nabla \psi_n'(\mathbf{r} - \mathbf{R}) d^3\mathbf{r} \tag{4.18}$$

The ∇ symbol without a subscript is the gradient with respect to $\mathbf{r}$, and I applied the fact that $\nabla_R = -\nabla$, when operating on a function of $(\mathbf{r} - \mathbf{R})$. But the final integral is $i/\hbar$ times the expectation value of momentum, in an eigenstate of the Hamiltonian $-(\hbar^2/2m)\nabla^2 + V$, which we know is zero. So

$$\langle \psi_n \mid \nabla_R \psi_n \rangle = -i \frac{q}{\hbar} \mathbf{A}(\mathbf{R}) \tag{4.19}$$

putt this into Berry's formula, we conclude that

$$\gamma_n(T) = \frac{q}{\hbar} \oint \mathbf{A}(\mathbf{R}) \cdot d\mathbf{R} = \frac{q}{\hbar} \int (\nabla \times \mathbf{A}) \cdot d\mathbf{a} = \frac{q\Phi}{\hbar} \tag{4.20}$$

it confirms the Aharonov-Bohm results.

Chapter 5

About the mono-pole Weyl semi-metal

Before we delve into the multi-Weyl semi metals and the properties of the Berry curvature in such material, we will first get a hand on monopole Weyl semimetals. Monopole Weyl semimetals represent a fascinating subset of topological materials that exhibit unique electronic properties governed by their Weyl nodes. These given materials are characterized by the presence of Weyl points in their electronic band structure, which act as monopoles of Berry curvature in momentum space. The interplay between the topological and physical characteristics of monopole Weyl semimetals opens up new pathways for advancements in quantum materials science.

5.1 Weyl Semimetals and the Concept of Monopoles

In Weyl semimetals, the conduction and valence bands touch at discrete points in the Brillouin zone, known as Weyl nodes. These nodes come in pairs with opposite chiralities (positive and negative monopole charges), dictated by the "no-monopole" theorem. Each node serves as source or sink from Berry curvature, a concept analogous to magnetic field lines emanating from a monopole in three-

dimensional space.

The Berry curvature field in momentum space around a Weyl node is mathematically described as:

$$\mathbf{\Omega}(\mathbf{k}) = \nabla \times \mathbf{A}(\mathbf{k}),$$

where $\mathbf{A}(\mathbf{k})$ is the Berry connection. The *Berry connection* is defined as:

$$\mathbf{A}(\mathbf{k}) = i\langle u(\mathbf{k})|\nabla_{\mathbf{k}}|u(\mathbf{k})\rangle$$

where: $|u(\mathbf{k})\rangle$ is the periodic part of the Bloch wavefunction (or the eigenstate of the Hamiltonian) at a point $\mathbf{k}$ in parameter space and $\nabla_{\mathbf{k}}$ is the gradient with respect to $\mathbf{k}$, the parameter space (e.g., crystal momentum).

The chirality (Chern number) of the Weyl nodes, given by the integral of Berry curvature over a surface enclosing the node, determines the monopole's "charge" ($+1$ or -1).

5.1.1 Chiral Partner of a Weyl Point

In a Weyl semimetal, the low-energy quasiparticles near Weyl points behaves like massless Weyl fermions, governed by the Weyl equation. A key feature of Weyl fermions is their chirality, which describes the handedness of the quasiparticle. Chirality is a fundamental property determined by whether the spin of the fermion is aligned or anti-aligned with its momentum. Weyl points in momentum space are characterized by a topological charge, often referred to as the *chirality* or *Chern number* of the point.

A Weyl point acts as a monopole in momentum space for Berry curvature, a gauge field associated with the Bloch wavefunctions of the electronic bands. The chirality of a Weyl point is quantified by the flux of the Berry curvature through surface enclosing the point, with a topological charge given by:

$$\chi = \pm 1. \tag{5.1}$$

Here, $\chi = +1$ corresponds to a Weyl point with positive chirality, while $\chi = -1$ corresponds to a Weyl point with negative chirality.

For a Weyl semimetal to exist, the net chirality over the entire Brillouin zone must be zero. This condition arises because the Weyl equation is derived from the Dirac equation, ensuring that Weyl points appear in pairs with opposite chirality everytime. Thus, every Weyl point with chirality $\chi = +1$ has a corresponding chiral partner with $\chi = -1$. These pairs of Weyl points are typically spaced in momentum space, with their separation determined by the breaking of inversion ($\mathcal{P}$) or time-reversal symmetry ($\mathcal{T}$).

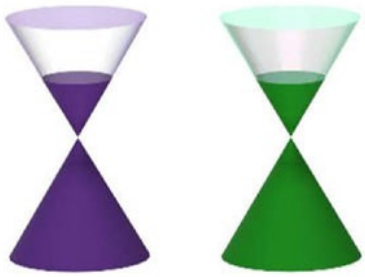

Figure 5.1: Chiral partner shown with band touching point

Fermi Arc Surface States

One key feature of Weyl semimetals is the presence of open surface-state band structures known as Fermi arcs.[10] These arcs connect projections of Weyl nodes with opposite chirality on the surface Brillouin zone, manifesting the topological nature of these materials.

Topology-Driven Transport Properties

- High mobility of charge carriers.
- Anomalous Hall and Nernst effects, linked to the Berry curvature's monopole structure.

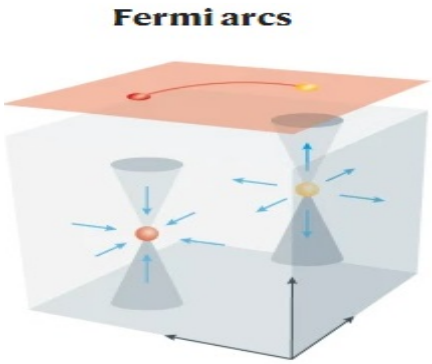

Figure 5.2: The Fermi arc connecting projection of monopole with positive and negative chirality.

Material Realizations

Materials like tantalum arsenide (TaAs), niobium arsenide (NbAs), and other transition-metal pnictides are prime candidates for Weyl semimetals. They exhibit well-separated Weyl nodes and clear Fermi arcs in experimental observations.

Chapter 6

Formulation of multi-Weyl semi-metal

6.1 Hamiltonian of a multi-Weyl semi-metal

To capture the special electronic properties of multi-Weyl semimetals, we begin with effective low-energy Hamiltonian that describes the band structure near a Weyl node. This Hamiltonian captures the essential characteristics of multi-Weyl nodes, where the topological charge m differentiates conventional Weyl points ($m = 1$) from higher-order, multi-Weyl nodes ($m \geq 2$). Near a multi-Weyl node, the Hamiltonian can be expressed as:

$$\mathcal{H}_0(\mathbf{k}) = \lambda \left(k_-^m \sigma_+ + k_+^m \sigma_- \right) + \hbar \eta v_z (k_z + \eta \kappa) \sigma_z, \tag{6.1}$$

where $k_\pm = k_x \pm i k_y$ and $\mathbf{k} = (k_x, k_y, k_z)$ is crystal momentum relative to Weyl node position at $\mathbf{k} = (0, 0, \eta\kappa)$. The parameters v_z and λ control the velocity and strength of Weyl point, while $\sigma_{x,y,z}$ are Pauli matrices describing the pseudo-spin degree of freedom, and $\eta = \pm$ distinguishes the chirality of Weyl node. The parameter m introduces a unique topological charge, leading to distinct Berry curvature and transport characteristics around multi-Weyl nodes, with a rotationally symmetric energy dispersion in the absence of tilting effects.

However, in real crystal structures with high-symmetry axes such as those with

C_2 or C_3 rotation symmetry Weyl points can develop additional anisotropy due to tilt effects,[7] which contribute strongly to the physical properties of the material. We counter this by including a tilt Hamiltonian term, which is a linear tilt along the k_z-axis and a quadratic tilt in the k_x-k_y plane:

$$\mathcal{H}_{\text{tilt}} = w_z k_{\parallel}^2 + w_z k_z. \tag{6.2}$$

The **linear tilt** term, $w_z k_z$, efficiently converts energy in the k_z direction, to a "tilted cone" configuration. Such a conversion breaks isotropy and generates extraordinary responses to external fields, perturbing transport and optical properties along the k_z-axis. At the same time, the **quadratic tilt** component, $w_z k_{\parallel}^2$, introduces a parabolic tilt in the k_x-k_y plane, modifying the energy dispersion depending on the rotational symmetry of the material. Combinatorially, these tilt words generalize the effective theory for multi-Weyl semimetals, enabling us to realistically describe symmetry and structural restrictions near Weyl points and build a better understanding of anisotropic phenomena, including direction-dependent transport and optical activity that arise from these tilts. The standard system parameters are listed in the table[6.1]

Table 6.1: Typical system parameters

Winding Number	w_z (eV$\AA$)	ccccc v_z (eV$\AA$)	$w_{\parallel}$ (eV$\AA^2$)	λ (eV$\AA^m$)
$m = 1$	0.5	1	0.03	0.4
$m = 2$	$(0 - 1.5)\ v_z$	1.5	$(0 - 0.25)\ \lambda$	0.2
$m = 3$	$(0 - 1.5)\ v_z$	2	$0 - 0.03$	0.04
$m = 4$	0.5	2.5	0.005	0.02
$m = 5$	0.3	3	0.005	0.01

The unique band structure of multi-Weyl semimetals as described by the Hamiltonian $\mathcal{H}_0 + \mathcal{H}_{\text{tilt}}$ is governed by the dispersion $E_{\eta,s}(\mathbf{k}) = w_z k_{\parallel}^2 + w_z k_z + s\sqrt{v_z^2(k_z + \eta\kappa)^2 + \lambda^2 k_{\parallel}^{2m}}$, with $s = \pm$ representing the conduction and valence band, respectively. The dispersion in the k_x-k_y plane around a node is anisotropic,

scaling as $k_{\parallel}^m$ (where $k_{\parallel} = \sqrt{k_x^2 + k_y^2}$), while along k_z, it remains linear. This leads to a power-law dependence in the density of states near the Weyl point, as well as distinct patterns in the Berry curvature. Such characteristics are experimentally accessible through techniques like angle-resolved photoemission spectroscopy (ARPES) and are central to understanding transport and response properties in multi-Weyl systems.

To obtain the eigenstates, we solve the eigenvalue problem $\mathcal{H}(\mathbf{k})|u_{\eta,s}(\mathbf{k})\rangle = E_s(\mathbf{k})|u_{\eta,s}(\mathbf{k})\rangle$, where $|u_{\eta,s}(\mathbf{k})\rangle$ are the Bloch eigenfunctions for the conduction ($s = +$) and valence ($s = -$) bands. These eigenfunctions are expressed as spinors that encode the chirality of the Weyl point. For a Weyl node of a given chirality, the Bloch eigenfunctions take the form:

$$|u_{\eta,s=+}(\mathbf{k})\rangle = \begin{pmatrix} \cos\frac{\zeta_\eta(\mathbf{k})}{2} \\ \sin\frac{\zeta_\eta(\mathbf{k})}{2} e^{mi\phi(\mathbf{k})} \end{pmatrix}, \tag{6.3}$$

and

$$|u_{\eta,s=-}(\mathbf{k})\rangle = \begin{pmatrix} \sin\frac{\zeta_\eta(\mathbf{k})}{2} \\ -\cos\frac{\zeta_\eta(\mathbf{k})}{2} e^{mi\phi(\mathbf{k})} \end{pmatrix}, \tag{6.4}$$

where $\cos\zeta_\eta = \eta v_z(k_z + \eta\kappa)/\sqrt{v_z^2(k_z + \eta\kappa)^2 + \lambda^2 k_{\parallel}^{2m}}$ and $\phi(\mathbf{k}) = \tan^{-1}(k_y/k_x)$ is the azimuthal angle in momentum space. These eigenfunctions carry a nontrivial Berry phase,[8] reflecting the topological properties of Weyl semimetals and leading to phenomena like the chiral anomaly and unique transport responses under external fields.

6.2 The Berry curvature field

The Bloch eigenfunctions play a crucial role in characterizing the topological structure of Weyl semimetals, as they encapsulate the Berry curvature a fundamental quantity for understanding the geometric phase and response to external fields.

Consequently, the eigenfunctions and their associated Berry curvature are central to the physical properties and experimental signatures of Weyl semimetals.

The Berry connection and Berry curvature are essential tools for exploring the geometric properties of quantum states within parameter space. For the given Hamiltonian $H(\mathbf{k})$ in Eq. (6.1), the Berry connection, [8, 9]

$$\mathbf{A}_\eta(\mathbf{k}) = i\langle u_{\eta,s=+}(\mathbf{k})|\nabla_\mathbf{k}|u_{\eta,s=+}(\mathbf{k})\rangle, \tag{6.5}$$

captures the phase information associated with adiabatic evolution in $\mathbf{k}$-space. Functionally similar to a vector potential in electromagnetism, the Berry connection provides a means to understand how the quantum phase accumulates due to the geometry of the state manifold. This framework has proven invaluable in examining systems with parameter-dependent Hamiltonians, revealing how adiabatic changes influence the quantum phase.[10]

The Berry field is derived from the Berry connection as

$$\begin{aligned}\mathbf{\Omega}^\eta_{m,s}(\mathbf{k}) &= \nabla_\mathbf{k} \times \mathbf{A}(\mathbf{k}) \\ &= \frac{\eta s}{4\pi}\left[\frac{m v_z \lambda^2 k_\parallel^{2m-1}}{(E_{\eta,+} - E_{\eta,-})^3}, 0, \frac{m^2 v_z \lambda^2 k_\parallel^{2m-2}(k_z + \eta\kappa)}{(E_{\eta,+} - E_{\eta,-})^3}\right]\end{aligned} \tag{6.6}$$

which acts as an effective magnetic field in momentum space. The closed surface integral $\chi = \oint_\mathcal{S} \mathbf{\Omega}^\eta_{m,-}(\mathbf{k}).d\mathcal{S} = -\eta m$, where $\mathcal{S}$ is the closed surface surrounding the Weyl nodes. Thus this field gives local insight into the geometrical structure of the quantum state manifold and often plays a key role in characterizing the multi-Weyl semimetals. The nature of this field for $m = 1, 2, 3$ about the Weyl nodes is shown in Fig. (7.1). Expectedly, the curvature of the fields becomes more pronounced for higher-order Weyl semi-metals, indicating the presence of more than one monopole.

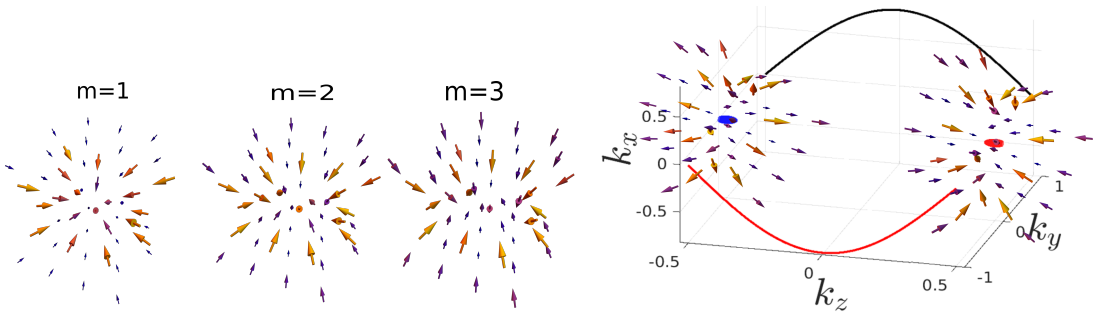

Figure 6.1: The upper panel shows the curvature of Berry fields that converge to the Weyl node for $m = 1$, $m = 2$ and $m = 3$. The lower panel shows the Fermi arc at $k_y = \pm 1$.

Chapter 7

Landau Levels and their degeneracy

7.1 Landau level

Landau levels belong to a set of distinct energy levels that an electron or any charged particle occupy when subjected to magnetic field. It comes from phenomena when charged particles like electrons move in a circular orbit in uniform magnetic field due to the Lorentz force. This term is in association with Lev Landau, the physicist who published it in 1930.

Magnetic Quantization: This process is called magnetic quantization, and it occurs when charged particles (for example, electrons) move in the presence of a magnetic field hesitated due to the magnetic field. Scientifically, when the electron is entering the magnetic field, due to its momentum, it has to move in a linear trajectory.

Degeneracy: Each Landau level has a large number of quantum states means (degeneracy), which depends on how strong magnetic field is. It is important in systems like the quantum Hall effect, where the number of available states will influences the behavior of the total system.

energy levels: When a free electron is placed in constant magnetic field, the energy levels are similar to

$$E_n = (n + \frac{1}{2})\hbar\omega_c \tag{7.1}$$

E_n is Landau level with index n being non-negative values. $\omega_c = \frac{eB}{m}$ is the cyclotron frequency, where e is charge, B is the magnetic field, and m is the charge mass.

Materials: There are many materials where Landau levels exist like Graphene, Two-Dimensional Electron Gas, Topological Insulators, High-Temperature Superconductors

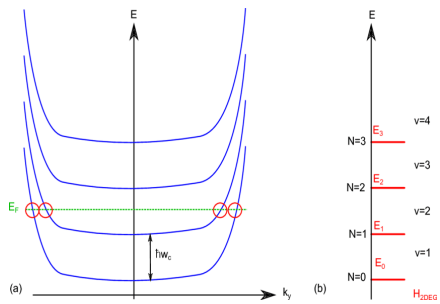

Figure 7.1: Landau levels

7.2 Landau level of gas

Hamiltonian of a free particle is

$$H_o = \frac{p^2}{2m}$$

When a particle is placed in magnetic field the Hamiltonian changes to

$$H = \frac{\pi^2}{2m} = \frac{(\vec{p} - q\vec{A})^2}{2m} \tag{7.2}$$

here $\vec{A}$ is the vector potential derived from magnetic field $\vec{B} = \vec{\nabla} \times \vec{A}$. We choose a

particular gauge known as Landau gauge $\vec{A} = B_o x\hat{y}$ for $\vec{B} = B_o\hat{z}$, the Hamiltonian becomes

$$H = \frac{p^2}{2m} - \frac{qB_o p_y}{m}x + \frac{q^2 B_o^2}{2m}x^2 \tag{7.3}$$

The particle is constrained to move on $x-y$ plane so we can write wave function in two parts

$$\psi_{p_y} = e^{\frac{ip_y y}{\hbar}}\phi_{p_y}(x), \text{where} \quad p_y = \hbar k_y \tag{7.4}$$

because Hamiltonian is invariant in y direction. The Schrodinger's equation

$$H\psi_{p_y} = E\left(p_y\right)\psi_{p_y}$$

will transform as

$$\left(\frac{p_x^2}{2m} + \frac{p_y^2}{2m} - \frac{qB_o p_y}{m}x + \frac{q^2 B_o^2}{2m}x^2\right)\phi_{p_y} = E\left(p_y\right)\phi_{p_y} \tag{7.5}$$

We define new terms $\ell_B^2 \equiv \frac{\hbar}{qB}$, and $\quad \omega_c \equiv \frac{|qB_o|}{m}$ and transform the Hamiltonian in complete squares

$$\frac{1}{2m}\left(p_x^2 + m^2\omega_c^2\left(x - k_y\ell_B^2\right)^2\right)\phi_{p_y} = E\left(p_y\right)\phi_{p_y} \tag{7.6}$$

it is like harmonic oscillator centered at $x = k_y\ell_B^2$ and it's energy levels given as

$$E_n = \hbar\omega_c\left(n + \frac{1}{2}\right) \tag{7.7}$$

these energy levels are known as Landau levels and ω_c is Cyclotron frequency.

For a given energy level for perticular n, every p_y corresponds to a state with same energy.

7.3 Degeneracy calculation

Let's say the sample dimension are given by $L_x \times L_y$ the separation in harmonic oscillator

$$\Delta x = \Delta k_y \ell_B^2 \tag{7.8}$$

it gives

$$\Delta x = \left(\frac{2\pi}{L_y}\right) \ell_B^2 \tag{7.9}$$

so total number of oscillator in system is

$$N = \frac{L_x}{\Delta x} = \frac{L_x L_y}{2\pi \ell_B^2} \tag{7.10}$$

where $\ell_B^2 \equiv \frac{\hbar}{qB}$ and after putting this in equation

$$N = \frac{B L_x L_y}{\hbar/e} = \frac{\phi}{\phi_o}. \tag{7.11}$$

Here N is the total flux, is gauge invariant because it is a physical quantity.

Chapter 8

Landau level calculation of hamiltonian

8.1 Hamiltonian of a multi-Weyl semi-metal

The Hamiltonian of a multi-Weyl semi-metal with tilt and without tilt combined is

$$\mathcal{H}_0 + \mathcal{H}_{\text{tilt}} = v_z k_z \sigma_z + \lambda \left(k_-^m \sigma_+ + k_+^m \sigma_- \right) + w_z k_z + w_\parallel k_\parallel^2 \tag{8.1}$$

here $\sigma_\pm = (\sigma_x \pm i\sigma_y)/2$ and $k_\parallel = \sqrt{k_x^2 + k_y^2}$. v_z and λ are real parameters. When a magnetic field is applied in z direction we can use Landau gauge for vector potential $\boldsymbol{A} = (0, Bx, 0)$. We transform the momentum to general momentum by $\boldsymbol{\Pi} = \boldsymbol{k} + e\boldsymbol{A}/\hbar$ in this gauge only y component is changed. We introduce new operators known as annihilation and creation operators

$$\hat{a} = \frac{l_B}{\sqrt{2}\hbar} \left(\Pi_x - i\Pi_y \right), \quad \hat{a}^\dagger = \frac{l_B}{\sqrt{2}\hbar} \left(\Pi_x + i\Pi_y \right) \tag{8.2}$$

The Hamiltonian will transform as

$$\begin{aligned} H =& w_z k_z + v_z k_z \sigma_z + \omega_{\parallel} \left(2\hat{a}^{\dagger}\hat{a} + 1\right) \\ &+ \lambda \left(\frac{\sqrt{2}}{l_B}\right)^m \left[\hat{a}^m \sigma_+ + \left(\hat{a}^{\dagger}\right)^m \sigma_-\right] \end{aligned}$$

here $l_B = \sqrt{\hbar/eB}$ is known as magnetic length and $\omega_{\parallel} = w_{\parallel}/l_B^2$.

8.2 Landau levels of the hamiltonian

For the Hamiltonian

$$\mathcal{H}_0 + \mathcal{H}_{\text{tilt}} = v_z k_z \sigma_z + \lambda \left(k_-^m \sigma_+ + k_+^m \sigma_-\right) + w_z k_z + w_{\parallel} k_{\parallel}^2 \tag{8.3}$$

the dispersion relation is

$$E_{\pm} = w_z k_z + w_{\parallel} k_{\parallel}^2 \pm \sqrt{v_z^2 k_z^2 + \lambda^2 k_{\parallel}^{2m}} \tag{8.4}$$

but when magnetic field is applied the energy levels are given by Landau levels

$$\text{En} = w_z \left(\frac{\eta\kappa}{2} + k_z\right) + \omega_{||}(-m + 2n + 1) - \sqrt{\frac{n!\tilde{\lambda}_m^2}{(n-m)!} + \left(\eta v_z \left(\frac{\eta\kappa}{2} + k_z\right) - m\omega_{||}\right)^2} \tag{8.5}$$

here we can write

$$\Gamma_n^m = \sqrt{\frac{n!\tilde{\lambda}_m^2}{(n-m)!} + \left(\eta v_z \left(\frac{\eta\kappa}{2} + k_z\right) - m\omega_{||}\right)^2} \tag{8.6}$$

here $\tilde{\lambda}_m = \left(\frac{\sqrt{2}\lambda}{l_B}\right)^m$ and the eigen wave function is

$$\begin{pmatrix} \alpha_n \phi_{n-m} \\ \beta_n \phi_n \end{pmatrix} \tag{8.7}$$

where α_n and β_n are calculated as

$$\alpha_n = \frac{\tilde{\lambda}_m \sqrt{\frac{n!}{(n-m)!}}}{\sqrt{\left(\left(\frac{\eta\kappa}{2} + k_z\right)\eta v_z - \frac{w_z \eta\kappa}{2} - m\omega_{||} + \Gamma_n^m\right)^2 + \tilde{\lambda}_m^2 \frac{n!}{(n-m)!}}} \tag{8.8}$$

$$\beta_n = \frac{\left(\left(\frac{\eta\kappa}{2} + k_z\right)\eta v_z - \frac{w_z \eta\kappa}{2} - m\omega_{||} + \Gamma_n^m\right)}{\sqrt{\left(\left(\frac{\eta\kappa}{2} + k_z\right)\eta v_z - \frac{w_z \eta\kappa}{2} - m\omega_{||} + \Gamma_n^m\right)^2 + \tilde{\lambda}_m^2 \frac{n!}{(n-m)!}}} \tag{8.9}$$

for $n \geq m$ and

$$E_n = \left(\frac{\eta\kappa}{2} + k_z\right)(w_z - \eta v_z) + (2n+1)\omega_{||} \tag{8.10}$$

eigen wave function is

$$\begin{pmatrix} 0 \\ \phi_n \end{pmatrix} \tag{8.11}$$

for $n \leq m$ where minimum value of n is zero. For plotting the Landau energy levels against k_z in Fig. 8.1 it comes out as tilted. Effect of linear and quadratic energy tilt is different. As we increased the number of Weyl points the tilt increases.

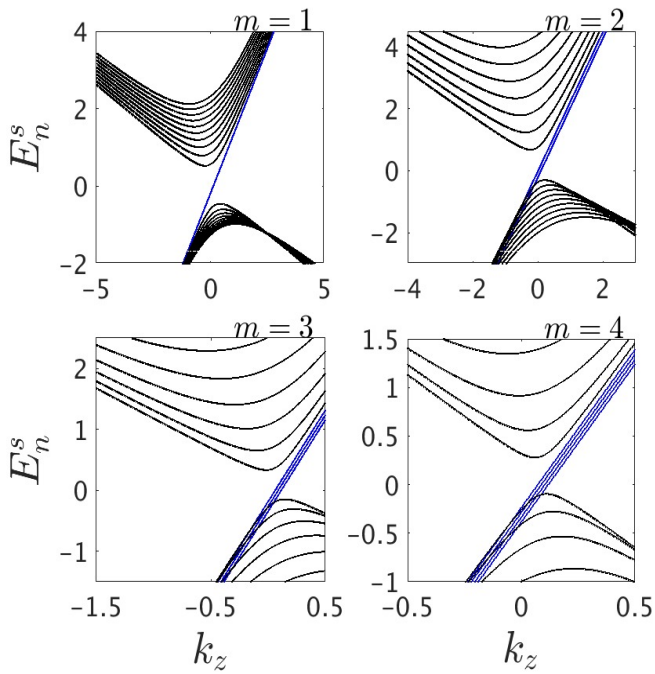

Figure 8.1: The plot shows tilted Landau levels for different values of m

Chapter 9

Chiral Anomaly

The chiral anomaly of Weyl semimetals (WSMs)[12] results from the underlying physical reason of these materials possessing an anomalous quantum phenomenon. WSMs have pairs of Weyl fermions with opposite chirality (handedness) as topological excitations. When electric field is applied parallel to a magnetic field (EB), the chiral symmetry of these fermions is broken, which leads to non-conservation law of chiral charge, which in turn leads to measurable transport phenomena.

- Negative Longitudinal Magnetoresistance (NLMR):[13, 11] The simplest realization of the chiral anomaly is the presence of negative longitudinal magnetoresistance when B and E are parallel. The phenomenon has been experimentally seen in several WSMs, such as TaAs, NaBi, and TaRhTe.

- Type-II Weyl Semimetals:[14, 15] In type-II WSMs, the Weyl cones are tilted, and a finite density of states appears at the Weyl points. The tilting impacts the manifestation of the chiral anomaly, and the NLMR becomes strongly anisotropic and relative to the E and B orientations.

- Thermal and Gravitational Effects: In addition to electrical transport, the chiral anomaly affects thermal behavior. Theory has anticipated and experiments have realized increased thermoelectric conductivity, Seebeck and

Nernst effects, and thermal conductivity in WSMs, with departures from classical regulations such as the Wiedemann-Franz law.

- Optical Detection of Chirality: Circularly polarized light can be used to directly probe the chirality of Weyl fermions. Optical detection is enabled by the measurement of chirality-sensitive photocurrents. This provides an in-situ, non-destructive means of accessing the chiral anomaly

9.1 Chiral anomaly of Landau levels

In Weyl semimetals, the low-energy excitations around the Weyl nodes can be represented as Weyl fermions with fixed chirality. When a magnetic field is introduced, Landau quantization takes place and results in discrete energy levels that are called Landau levels. The zeroth Landau level (n = 0) has linear dispersion along the direction of the magnetic field, which is a characteristic of Weyl fermions.

The chiral anomaly occurs when electric and magnetic fields are parallel to one another $E||B$. This orientation causes the chiral charge to be violated, leading to an inequality of populations between Landau levels with opposite chirality. This discrepancy is experienced as a negative longitudinal magnetoresistance (NLMR) and is a clear indication of the chiral anomaly.

Chapter 10

Conclusion

We calculated the eigenfunction for a specific Hamiltonian and calculated its Berry curvature and took its integration around the field source point which gave the topological charge. It comes from conduction and valence band touching in momentum space.

We transformed the Hamiltonian for easier calculation of Landau levels, and it shows similarity to harmonic oscillator from quantum mechanics. And we calculated its eigenfunction and eigenvalues for plotting.

Landau levels of multi-Weyl Hamiltonian for m number of Weyl points is calculated. It is different for energy levels larger than m values and for lesser than that. Landau levels graph are plotted as E_n on y axis and k_z on x axis for different values of m from one to four, and for different n values. We will use different values of parameter to see how Landau tilt changes.

For different values of m the number of straight lines is different it is sam as m values.

We have studied the nonlinear Landau Levels in multi-Weyl semimetal which show deviations from the standard linear dependence observed in conventional semimetals.

Bibliography

[1] Fang, C., Gilbert, M. J., Dai, X., & Bernevig, B. A. "Multi-Weyl Topological Semimetals Stabilized by Point Group Symmetry." Physical Review Letters, **108(26)**, 266802, (2012).

[2] Liu, J., Zunger, A., Rappe, A. M. "Higher-order Weyl semimetals: Topological properties and response functions." Physical Review B, **107(8)**, 085146 (2023).

[3] Dantas, R. M. A., Basu, B. "Anisotropic transport and Berry curvature dipole in multi-Weyl semimetals." Journal of Physics: Condensed Matter, **33(37)**, 375501 (2021).

[4] Armitage, N. P., Mele, E. J., & Vishwanath, A. "Weyl and Dirac semimetals in three-dimensional solids." Reviews of Modern Physics, **90(1)**, 015001 (2018).

[5] Zyuzin, A. A., & Burkov, A. A. "Topological response in Weyl semimetals and the chiral anomaly." Physical Review B, **86(11)**, 115133 (2012).

[6] Yan, B., Felser, C. "Topological Materials: Weyl Semimetals." Annual Review of Condensed Matter Physics, **8(1)**, 337-354 (2017).

[7] Goerbig, M. O., & Montambaux, G. "Tilted anisotropic Dirac cones in quinoid-type graphene and -(BEDT-TTF)$_2$I$_3$." Physical Review B, **78(4)**, 045415 (2008).

[8] Resta, R., "Berry Phase in Electronic Wavefunctions," Journal of Physics: Condensed Matter, **12**, R107-R143, (2000).

[9] Xiao, D., Chang, M.-C., and Niu, Q., "Berry phase effects on electronic properties," Reviews of Modern Physics, **82**, 1959-2007, (2010).

[10] Huang, S. M. et al. A Weyl fermion semimetal with surface Fermi arcs in the transition metal monopnictide TaAs class. Nat. Commun. 6, 7373 (2015).

[11] Huang, X. et al. Observation of the chiral-anomaly-induced negative magnetoresistance in 3D Weyl semimetal TaAs. Phys. Rev. X 5, 031023 (2015).

[12] Xiong, J. et al. Evidence for the chiral anomaly in the Dirac semimetal Na3Bi. Science 350, 413 (2015).

[13] Li, Y. et al. Negative magnetoresistance in Weyl semimetals NbAs and NbP: intrinsic chiral anomaly and extrinsic effects. Front. Phys. 12, 127205 (2016).

[14] T. E. O'Brien, M. Diez, and C. W. J. Beenakker, Magnetic Breakdown and Klein Tunneling in a Type-II Weyl Semimetal, Phys. Rev. Lett. 116, 236401 (2016).

[15] K. Halterman and M. Alidoust, Waveguide modes in Weyl semimetals with tilted dirac cones, Opt. Express 27, 36164 (2019).